IEEE Access
Multidisciplinary | Rapid Review | Open Access Journal

Received August 2, 2019, accepted September 13, 2019, date of publication September 24, 2019, date of current version October 8, 2019.

Digital Object Identifier 10.1109/ACCESS.2019.2943538

Frequency-Based Decentralized Conservation Voltage Reduction Incorporated Into Voltage-Current Droop Control for an Inverter-Based Islanded Microgrid

HYEON-JIN MOON[1], (Student Member, IEEE), YOUNG-JIN KIM[2], (Member, IEEE), AND SEUNG-IL MOON[1], (Senior Member, IEEE)

[1]School of Electrical Engineering and Computer Science, Seoul National University, Seoul 08826, South Korea
[2]Department of Electrical Engineering, Pohang University of Science and Technology, Pohang 37673, South Korea

Corresponding author: Young-Jin Kim (powersys@postech.ac.kr)

This work was supported in part by the Human Resources Development Program of Korea Institute of Energy Technology Evaluation and Planning (KETEP), granted financial resource from the Ministry of Trade, Industry and Energy, Republic of Korea, under Grant 20194030202420, and in part by the Korea Institute of Energy Technology Evaluation and Planning (KETEP) grant funded by the Korea Government (MOTIE) under Grant 70300037.

ABSTRACT Conservation voltage reduction (CVR) aims to decrease load demands by regulating bus voltages at a low level. This paper proposes a new strategy for decentralized CVR (DCVR), incorporated into the current-based droop control of inverter-interfaced distributed energy resources (IDERs), to improve the operational reliability of an islanded microgrid. An I_{dq} controller is developed as an outer feedback controller for each IDER, consisting of I_d–V controllers for the DCVR and I_d–ω and I_q–V controllers for power sharing. In particular, the I_d–V controllers adjust the output voltages of the IDERs in proportion to the frequency variation determined by the I_d–ω controllers. This enables the output voltages to be reduced by the same amount, without communication between the IDERs. The I_q–V controllers are responsible for reactive power sharing by adjusting the voltages while taking into account the I_d–V controllers. Small-signal analysis is used to verify the performance of the proposed DCVR with variation in the I_d–ω and I_q–V droop gains. Case studies are also carried out to demonstrate that the DCVR effectively mitigates an increase in the load demand, improving the operational reliability, under various load conditions determined by power factors and load compositions.

INDEX TERMS Current-based droop control, decentralized conservation voltage reduction, distributed energy resources, microgrid, operational reliability, small-signal analysis.

I. INTRODUCTION

Microgrids (MGs) are self-contained local entities including distributed energy resources (DERs) and loads [1]. One particular focus of the ongoing development of MG- and device-level controllers is to improve the reliability of the system, i.e., the ability to balance between power generation and load demand, so that frequency and voltages can be maintained within acceptable ranges when MGs operate in islanded mode [2]. Meanwhile, power converters have been widely used as the interfaces for DERs, so that they can be connected to islanded MGs. Inverter-interfaced DERs (IDERs) have faster time responses than conventional synchronous generators. Therefore, IDERs have recently received significant attention due to their potential for improving, for example, real-time frequency and voltage stability, power quality, and fault-current coordination in islanded MGs [3]–[5]. Moreover, IDERs are capable of operating as grid-forming units, similar to synchronous generators, determining the frequency and bus voltages in an islanded MG. An MG with grid-forming IDERs is called an inverter-based MG [6], [7].

Many studies were carried out on the real-time control of DERs, aiming to improve the operational stability of islanded MGs. For example, in [8]–[12], centralized control schemes were implemented in an MG central controller or an MG energy management system to achieve cooperation between

The associate editor coordinating the review of this manuscript and approving it for publication was Madhav Manjrekar.

DERs, controllable loads, and voltage-regulating devices such as capacitor banks. These centralized schemes have advantages in terms of determining global or near-global optimal operations of MGs, based on full observation of the operating conditions of DERs. However, a large amount DER-related data must be transferred in real time via communications links, making it difficult to implement such centralized schemes in practice [5].

To overcome this difficulty, decentralized control schemes have been discussed in several studies (e.g., [13]–[24]), where coordination between individual DERs is achieved using device-level controllers based on local measurements. For example, the P–ω and Q–V droop control schemes have been widely adopted [13]–[17], so that the total power generation can be shared among the DERs for real-time frequency and voltage regulations. The conventional droop control schemes have several drawbacks with regard to stability margin and transient response, which are particularly important to islanded MGs [10]. Therefore, various modifications of the droop control schemes have been discussed in [18]–[24], for example using virtual impedance and V–I droop controllers to improve the P–Q decoupling and power sharing accuracy.

Meanwhile, conservation voltage reduction (CVR) is a well-known technique to reduce energy consumption and peak demands by maintaining network voltages at a low level [25]–[31]; the application and assessment of CVR was comprehensively presented in [28]. Recently, the CVR technique has been revisited to mitigate the lack of power and energy supplies particularly in islanded MGs [32]–[34]. For example, in [32], the output voltages of synchronous machine-based DERs at the point of common coupling (PCC) were controlled by using MG frequency deviation as a common input signal for the proportional-integral (PI) controllers of the exciters. The other DERs located at different buses operated as slave units to supply the pre-determined active power, regardless of the PCC voltage. In [33], the decentralized CVR (DCVR) approach was implemented using V–I droop control of the IDERs in an islanded MG. However, the voltage reduction became large under light loading conditions, when the load demand reduction was not much required. On the contrary, the DCVR was rather limited under heavy loading conditions, when the load reduction was more valuable. In [34], coordination between DCVR and load shedding was discussed using P–ω and Q–V droop controllers for inverter-based MGs. A DCVR strategy was implemented based on the variation in the apparent output power of each IDER, leading to different extents of voltage reduction at each bus when the IDERs operated under different droop coefficients and/or power ratings. Moreover, for the DCVR approaches discussed in [32]–[34], the small-signal stability needs to be investigated in more detail before they can be applied in practical situations.

In this paper, we propose a new DCVR strategy for IDERs that incorporates current-based droop controllers for power sharing in inverter-based islanded MGs. Specifically, for the proposed strategy, an I_{dq} controller is developed as an outer feedback controller for each IDER; therefore, it can be readily integrated into an existing IDER. The I_{dq} controller consists of two modules: I_d–V control for DCVR and the I_d–ω and I_q–V control for power sharing. The I_d–V controllers adjust the output voltage of IDERs in proportion to the MG frequency variation (or, equivalently, the load demand variation), which is mainly determined by the I_d–ω droop coefficients. Hence, the reductions in bus voltages become large under heavy loading conditions. Moreover, as the frequency is a global signal in the MG, this enables the individual IDERs to reduce their output voltage by the same amount in a decentralized manner: i.e., without relying on communication between IDERs. Considering the I_d–V controllers, the I_q–V controllers induce additional variations in the output voltage of the IDERs for reactive power sharing, depending on the I_q–V droop coefficients; the resulting output voltages need to be maintained within an acceptable range for time-varying load demand. Note that the I_d–$\omega$and I_q–V droop controllers can replace the conventional P–ω and Q–V droop controllers, eliminating time delay in the measurements of P and Q. Therefore, the current-based controllers enable the IDERs to respond faster than conventional controllers, thus improving their transient responses.

Small-signal analysis is performed using the state-space model of the inverter-based MG for various coefficients of the I_{dq} controller, to verify that the proposed DCVR increases the system damping and improves the MG operational reliability. Simulation case studies are also carried out to validate that the proposed DCVR improves the transient response of the IDERs and enables regulation of bus voltages at the lower level, further reducing the load demand, under various load conditions, which are characterized by load power factors and compositions.

II. DESCRIPTION OF MG TEST BED AND PROPOSED DCVR

In this paper, a three-bus inverter-based MG [6], [35] is used as a test bed to develop and analyze the proposed DCVR strategy. Fig. 1 shows the MG configuration and Table 1 lists the load impedances and line parameters. Specifically, the MG includes three IDERs, each of which is equipped with a local controller and acts as a grid-forming unit. In other words, the IDERs determine MG frequency and voltage according to a multi-master approach while maintaining the balance between generation and load demand in real time. As shown in Fig 1, the MG also contains a variable load that operates as a grid-following unit: i.e., its input power is adjusted based on the bus voltage v_{b2}. Similarly, the power inputs of two constant impedance loads vary depending on bus voltages v_{b1} and v_{b3}.

A. VOLTAGE DEPENDENCE OF LOADS AND MG-FORMING OF IDERS

A static load model, discussed in [36], is adopted to represent the active and reactive power demands (i.e., P_{Load} and Q_{Load},

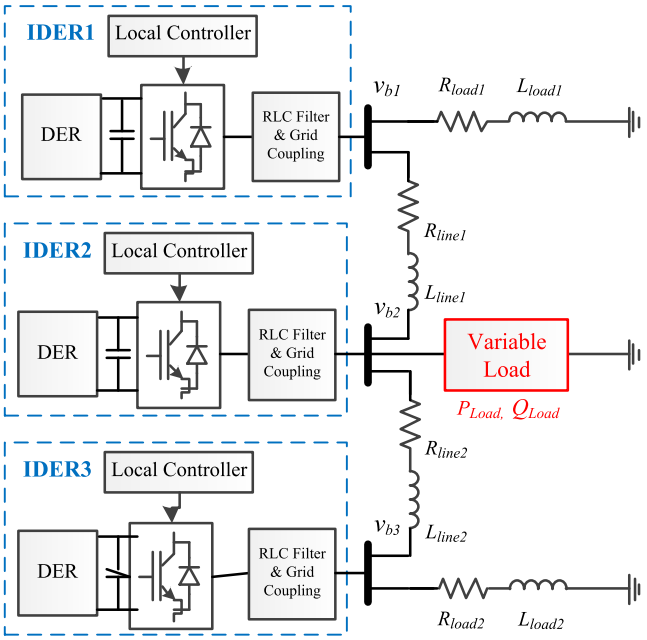

FIGURE 1. An islanded MG including IDERs and voltage-dependent loads.

TABLE 1. Load impedances and line parameters in the MG test bed.

Parameters	Values	Parameters	Values
R_{load1}	25 Ω	L_{load1}	10 nH
R_{load2}	20 Ω	L_{load2}	10 nH
R_{line1}	0.23 Ω	L_{line1}	0.3 mH
R_{line2}	0.35 Ω	L_{line2}	1.8 mH

respectively) of the variable load for the actual bus voltage V as:

$$P_{Load} = P_0 \frac{\omega_l}{s+\omega_l}\left(\frac{V}{V_0}\right)^{n_p},$$
$$Q_{Load} = Q_0 \frac{\omega_l}{s+\omega_l}\left(\frac{V}{V_0}\right)^{n_q}, \quad (1)$$

where P_0 and Q_0 are the active and reactive load demands, respectively, at the rated voltage V_0. Moreover, n_p and n_q are the voltage exponents for the active and reactive power, respectively, which are determined based on the inherent characteristics of the load. In (1), ω_l is the cut-off frequency of the first-order low-pass filter (LPF) that reflects the transient load response [37]. Note that (1) can be expressed equivalently using ZIP coefficients [36].

As shown in Fig. 2, the IDER is a general type of a DER, such as a fuel cell, battery, or micro-turbine, which is connected to the network via a voltage source inverter (VSI). The VSI interface changes the DC output voltage from the DER to the AC voltage for the grid. An RLC filter is also required to ensure a low ripple current on the grid side and set the resonant frequency at the desired value [6]. The local controller of the IDER includes an outer feedback loop for the power (or I_{dq}) controller, which determines the voltage and frequency

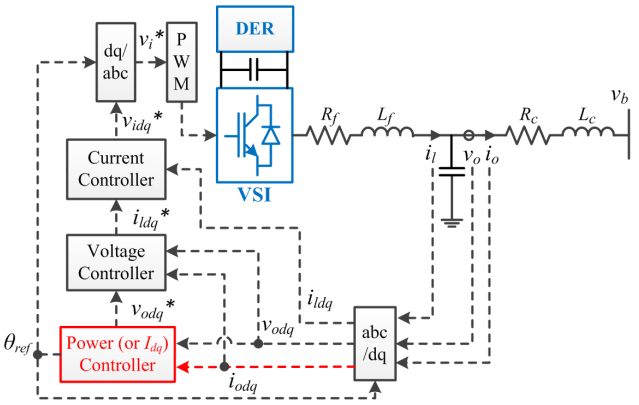

FIGURE 2. Schematic diagram of a VSI-interfaced DER and its local controller including the outer and inner feedback loops. The RLC filter and grid coupling impedance are also presented.

references required for real-time balance between the total generation and load demand. It also contains nested feedback loops for the voltage and current controllers, to ensure that the actual voltage and current v_{odq} and i_{ldq}, respectively, successfully follow the reference values, which are $v_{odq}{}^*$ and $i_{ldq}{}^*$, respectively.

The power controller aims for power sharing among IDERs using droop control schemes. In a conventional scheme, the P–ω and Q–V droop controllers are implemented using the coefficients m_P and n_Q, respectively, as:

$$\omega^* = \omega_n - m_P P, \quad (2)$$
$$v_{od}^* = V_n - n_Q Q, \quad v_{oq}^* = 0, \quad (3)$$

where ω^* and ω_n are the references and nominal set points, respectively, of the MG frequency and v_{od}^* and V_n are those of the d-axis output voltage of the IDER. Furthermore, P and Q represent the low-frequency components of the instantaneous active and reactive power, respectively, which are measured at the output ports of the LPFs in the power controller as:

$$P = \frac{\omega_c}{s+\omega_c} p_{ins}, \quad Q = \frac{\omega_c}{s+\omega_c} q_{ins}, \quad (4)$$
$$p_{ins} = v_{od} i_{od} + v_{oq} i_{oq}, \quad q_{ins} = v_{oq} i_{od} - v_{od} i_{oq}, \quad (5)$$

where v_{od}, v_{oq}, i_{od} and i_{oq} are the dq-axis output voltages and currents of the IDER, respectively. Moreover, ω_c is the cut-off frequency of the LPF.

B. FREQUENCY-BASED DCVR WITH CURRENT-BASED DROOP CONTROL

Fig. 3 shows a block diagram of the proposed I_{dq} controller, where the I_d–V controller reduces the output voltage of the IDER for the frequency-based DCVR in coordination with the current-based droop controllers (i.e., I_d–ω and I_q–V), for active and reactive power sharing. Specifically, the proposed I_{dq} controller operates on the voltage-oriented dq-reference frame where v_{od} only has DC component and v_{oq} is set to zero. From (5), p_{ins} and q_{ins} can then be expressed as:

$$p_{ins} = v_{od} i_{od}, \quad q_{ins} = -v_{od} i_{oq}. \quad (6)$$

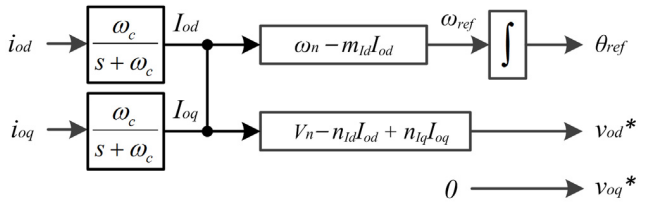

FIGURE 3. Block diagram of the proposed I_{dq} controller for frequency-based DCVR incorporated into the current-based droop control for power sharing.

As v_{od} is close to the rated value (i.e., 1 pu) under normal operating conditions of the IDER, p_{ins} and q_{ins} can mainly be controlled based on i_{od} and i_{oq}, respectively. The conventional (i.e., P–ω and Q–V) droop controllers, shown in (2) and (3), can then be replaced by the dq-axis current-based droop controllers as:

$$\omega^* = \omega_n - m_{Id} I_{od}, \tag{7}$$

$$v_{od}^* = V_n + n_{Iq} I_{oq}, \quad v_{oq}^* = 0, \tag{8}$$

where I_{od} and I_{oq} are the low-pass-filtered values of i_{od} and i_{oq}, respectively, as shown in Fig. 3. In (7) and (8), m_{Id} and n_{Iq} are the corresponding droop coefficients. Compared to (2) and (3), the current-based droop controllers, (7) and (8), can respond to variations in the load demand faster, mainly due to the shorter time delay in the measurement, which is beneficial for improving the stability of the frequency and voltage of the MG [20].

For integration with (7) and (8), the I_d–V controller for the proposed DCVR is implemented in the form of a droop controller as follows:

$$v_{od}^* = V_n - n_{Id} I_{od} + n_{Iq} I_{oq}, \tag{9}$$

where n_{Id} is the DCVR coefficient for the relationship between I_{od} and v_{od}. As the total load demand in the MG increases, the power outputs p_{ins} and, consequently, the current output i_{od} of the IDERs, increase according to (7) for MG frequency regulation: i.e., to maintain the instantaneous balance of active power. This leads to a decrease in v_{od}^* (and v_{od}), as shown in (9), reducing the power consumption of the voltage-dependent loads and mitigating the increase in total load demand. In other words, the IDERs participate in both DCVR and active power sharing. Incorporation of the I_d–V controller into current-based droop controllers enables the individual IDERs to adjust their output voltages by the same amount in a decentralized manner, while monitoring the MG frequency, as discussed in Section II-C. DCVR can be achieved without communication between IDERs, because the frequency is a global signal in the MG. Moreover, the larger the increase in load demand, the larger the reduction of bus voltages that can be achieved, because the MG frequency deviation is proportional to the load demand variation for fixed I_d–ω droop coefficients.

C. ΔV_{DCVR} WITH RESPECT TO DCVR COEFFICIENTS n_{Id} AND k_{DCVR}

Given the local measurements and controllers, we adopted a simple and effective approach to determine n_{Id} in (9), so that the output voltages of the IDERs are reduced while maintaining the overall profile of the original bus voltages in the MG. In other words, the output voltage drops of the IDERs with an increase in load demand are set equal to each other, as follows:

$$\Delta V_{DCVR} = -n_{Id1} I_{od1} = \cdots = -n_{Idi} I_{odi} = \cdots = -n_{Idn} I_{odn}. \tag{10}$$

For IDER unit i, (10) can be satisfied by using the frequency deviation $\Delta\omega = \omega^* - -\omega_n = -m_{Id} \cdot I_{od}$, as:

$$\Delta V_{DCVR} = -n_{Idi} I_{odi} = k_{DCVR} \Delta\omega = -k_{DCVR} m_{Idi} I_{odi}, \quad \forall i, \tag{11}$$

where k_{DCVR} is defined as the DCVR coefficient related to the sensitivity of ΔV_{DCVR} to $\Delta\omega$. Based on (6)–(10), (11) can be expressed equivalently as:

$$\Delta V_{DCVR} = k_{DCVR} \Delta\omega = -k_{DCVR} \frac{\Delta P_D}{\sum_{i=1}^{n} \left(v_{odi\_ss} / m_{Idi} \right)}, \tag{12}$$

where ΔP_D is the variation in the total load demand and v_{odi_ss} is the steady state value of v_{odi}. This verifies that the proposed method allows individual IDERs to reduce their output voltages by the same amount for the DCVR, in proportion to the variation in the MG frequency or the net load demand, even in the general case where the IDERs have power ratings, steady-state voltages, and droop coefficients. It is possible to determine the optimal values of n_{Idi} and ΔV_{DCVRi} for the individual IDERs; this task is left for future work. Note that the resulting output voltages of the IDERs are determined not only by ΔV_{DCVR} but also by the I_q–V droop controller for the reactive power sharing. Therefore, an adaptive approach to determining n_{Id} or k_{DCVR}, in coordination with voltage regulating devices, will also be worth investigating in future research.

III. SMALL SIGNALANALYSIS OF PROPOSED DCVR STRATEGY

A. STATE-SPACE MODELING OF THE MG TEST BED

A complete state-space model of the MG test bed, shown in Fig. 1, is established to analyze the small-signal stability for the proposed DCVR strategy. The modeling is achieved by dividing the entire MG into three modules: the IDERs, loads, and network lines. Apart from the proposed I_{dq} controller, shown in Fig. 3, the state-space model is implemented mainly based on [6] and [35]. For example, each IDER operates on an individual dq-reference frame rotating at a given angular frequency, which is set by its local controller. For simple representation, the dq-axis variables Δx_d and Δx_q are aggregated as $\Delta x_{dq} = [\Delta x_d, \Delta x_q]^T$. The combination of the state variables is represented simply as $[\Delta x] = [\Delta x_1, \Delta x_2, \cdots, \Delta x_m]^T$.

1) MODELING IDERS WITH THE PROPOSED I_{DQ} CONTROLLER

The proposed I_{dq} controller can be modelled as:

$$\begin{bmatrix} \dot{\Delta\delta} \\ \Delta I_{od} \\ \Delta I_{oq} \end{bmatrix} = \underbrace{\begin{bmatrix} 0 & -m_{Id} & 0 \\ 0 & -\omega_c & 0 \\ 0 & 0 & -\omega_c \end{bmatrix}}_{\mathbf{A_P}} \begin{bmatrix} \Delta\delta \\ \Delta I_{od} \\ \Delta I_{oq} \end{bmatrix} + \underbrace{\begin{bmatrix} -1 \\ 0 \\ 0 \end{bmatrix}}_{\mathbf{B_{P\omega}}} \Delta\omega_{com} + \underbrace{\begin{bmatrix} 0 & 0 & 0 & 0 & 0 & 0 \\ 0 & 0 & 0 & 0 & \omega_c & 0 \\ 0 & 0 & 0 & 0 & 0 & \omega_c \end{bmatrix}}_{\mathbf{B_P}} \begin{bmatrix} \Delta i_{ldq} \\ \Delta v_{odq} \\ \Delta i_{odq} \end{bmatrix}, \tag{13}$$

$$\begin{bmatrix} \Delta\omega^* \\ \Delta v_{od}^* \\ \Delta v_{oq}^* \end{bmatrix} = \underbrace{\overbrace{\begin{bmatrix} 0 & -m_{Id} & 0 \\ 0 & -n_{Id} & n_{Iq} \\ 0 & 0 & 0 \end{bmatrix}}^{\mathbf{C_{P\omega}}}}_{\mathbf{C_{Pv}}} \begin{bmatrix} \Delta\delta \\ \Delta I_{od} \\ \Delta I_{oq} \end{bmatrix} = \mathbf{C_P} \begin{bmatrix} \Delta\delta \\ \Delta I_{od} \\ \Delta I_{oq} \end{bmatrix}, \tag{14}$$

where δ is the angular difference between the common reference frame and the reference frame of an individual inverter, both of which rotate at the speed of ω_{com}. The I_{dq} controller model in (13) and (14) is then integrated with the models of the voltage and current controllers, the *RLC* filter, and the coupling impedance to establish a model of an IDER as:

$$[\dot{\Delta x_{INVi}}] = \mathbf{A_{INVi}}[\Delta x_{INVi}] + \mathbf{B_{INVi}}\left[\Delta v_{bDQi}\right] + \mathbf{B_{INV\omega i}}\Delta\omega_{com}, \tag{15}$$

$$\left[\Delta\omega_i \quad \Delta i_{oDQi}\right]^T = \left[\mathbf{C_{INV\omega i}} \quad \mathbf{C_{INVci}}\right]^T [\Delta x_{INVi}], \tag{16}$$

where

$$[\Delta x_{INVi}] = [\Delta\delta_i \ \Delta I_{odi} \ \Delta I_{oqi} \ \Delta\varphi_{dqi} \ \Delta\gamma_{dqi} \ \Delta i_{ldqi} \ \Delta v_{odqi} \ \Delta i_{odqi}]^T. \tag{17}$$

The coefficient matrices $\mathbf{A_{INVi}}$, $\mathbf{B_{INVi}}$, $\mathbf{B_{INV\omega i}}$, $\mathbf{C_{INV\omega i}}$, and $\mathbf{C_{INVci}}$ in (15) and (16) are provided in the Appendix. In (17), $\Delta\varphi_{dqi}$ and $\Delta\gamma_{dqi}$ are the state variables related to the PI controllers in the voltage and current controllers, shown in Fig. 2. Note that the input and output variables in the individual reference frames have been transformed to those in the common frame, which are represented by the subscript of *DQ* in (15) and (16), as:

$$\left[\Delta i_{oDQi}\right] = \mathbf{T_{Si}}\left[\Delta i_{odqi}\right] + \mathbf{T_{Ci}}[\Delta\delta_i], \tag{18}$$

$$\left[\Delta v_{bdqi}\right] = \mathbf{T_{Si}^{-1}}\left[\Delta v_{bDQi}\right] + \mathbf{T_{Vi}^{-1}}[\Delta\delta_i], \tag{19}$$

where the transformation matrices $T_{\mathbf{Si}}$, $T_{\mathbf{Ci}}$, and $T_{\mathbf{Vi}}$ are presented in the Appendix. The transformation enables the individual IDER models to be combined, as follows:

$$[\dot{\Delta x_{INV}}] = \mathbf{A_{INV}}[\Delta x_{INV}] + \mathbf{B_{INV}}\left[\Delta v_{bDQ}\right], \tag{20}$$

$$\left[\dot{\Delta i_{oDQ}}\right] = \mathbf{C_{INVc}}[\Delta x_{INV}], \tag{21}$$

where $\mathbf{A_{INV}}$, $\mathbf{B_{INV}}$, and $\mathbf{C_{INVc}}$ are also defined in the Appendix.

2) MODELING THE NETWORK WITH LOADS AND IDERS

While focusing on the analysis of the proposed I_{dq} controllers, we adopt general types of RL branches and loads from [6] and [35] for simplicity as:

$$\left[\dot{\Delta i_{lineDQ}}\right] = \mathbf{A_{NET}}\left[\Delta i_{lineDQ}\right] + \mathbf{B_{1NET}}\left[\Delta v_{bDQ}\right] + \mathbf{B_{2NET}}\Delta\omega, \tag{22}$$

$$\left[\dot{\Delta i_{loadDQ}}\right] = \mathbf{A_{LOAD}}\left[\Delta i_{loadDQ}\right] + \mathbf{B_{1LOAD}}\left[\Delta v_{bDQ}\right] + \mathbf{B_{2LOAD}}\Delta\omega, \tag{23}$$

where $\mathbf{A_{NET}}$, $\mathbf{A_{LOAD}}$, $\mathbf{B_{1NET}}$, $\mathbf{B_{2NET}}$, $\mathbf{B_{1LOAD}}$, and $\mathbf{B_{2LOAD}}$ depend on the network topology, line parameters, load impedances, and line and load currents in the steady state; the specific elements can be found in [6]. In (20)–(23), the *DQ*-axis bus voltages $[\Delta v_{bDQ}]$ are treated as common inputs to the models of the IDERs, lines, and loads. Assuming a large virtual resistor r_N between each bus and ground, $[\Delta v_{bDQ}]$ is related to the *DQ*-axis currents of the IDERs, lines, and loads as:

$$\left[\Delta v_{bDQ}\right] = \mathbf{R_N}\left(\mathbf{M_{INV}}[\Delta i_{oDQ}] + \mathbf{M_{NET}}[\Delta i_{lineDQ}] + \mathbf{M_{LOAD}}[\Delta i_{loadDQ}]\right), \tag{24}$$

where $\mathbf{R_N}$ is the diagonal matrix representing r_N. Moreover, $\mathbf{M_{INV}}$, $\mathbf{M_{NET}}$, and $\mathbf{M_{LOAD}}$ are the mapping matrices used to account for the connections between the IDERs, lines, and loads, respectively, in the MG. Using (24), the state-space models (20), (22), and (23) are integrated into the complete model of the MG test bed as:

$$\begin{bmatrix} \dot{\Delta x_{INV}} \\ \dot{\Delta i_{lineDQ}} \\ \dot{\Delta i_{loadDQ}} \end{bmatrix} = \mathbf{A_{MG}} \begin{bmatrix} \Delta x_{INV} \\ \Delta i_{lineDQ} \\ \Delta i_{loadDQ} \end{bmatrix}, \tag{25}$$

where the system state matrix $\mathbf{A_{MG}}$ is presented in the Appendix.

B. SMALL-SIGNAL STABILITY ANALYSIS USING EIGENVALUES

The small-signal stability of the proposed DCVR is analyzed using the state-space model (25) of the MG. For simplicity, the IDERs in the MG are assumed to be identical. Table 2 lists the parameters of the MG model, determined mainly based on [6], under normal operating conditions with fixed load demand. Note that n_{Id} is set to 5% at the rated current for

TABLE 2. MG test bed parameters.

Parameters		Values	Parameters		Values
f	[Hz]	50	m_P	[rad/s/W]	9.40e–5
L_f	[mH]	1.35	n_Q	[V/Var]	1.27e–3
R_f	[Ω]	0.1	m_{Id}	[V/A]	3.59e–2
C_f	[μF]	50	n_{Id}	[V/A]	2.42e–1
L_c	[mH]	0.35	n_{Iq}	[V/A]	7.26e–1
R_c	[Ω]	0.03	K_{pv}		0.05
ω_c	[rad/s]	31.41	K_{iv}		390
r_N	[Ω]	1000	K_{pc}		10.5
F		0.75	K_{ic}		16e3

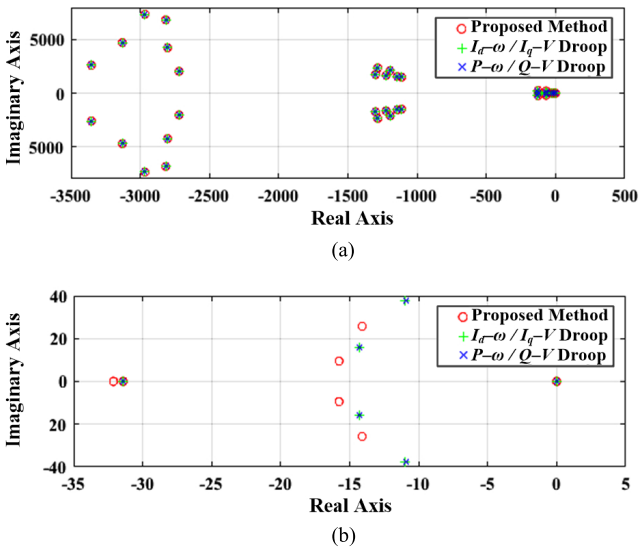

FIGURE 4. (a) Three eigenvalue clusters for the proposed DCVR, current-based droop control, and conventional droop control strategies, and (b) close-up plots for the eigenvalues in the rightmost cluster.

a rated power of 10 kW and voltage of 380 V. Fig. 4 shows the eigenvalues of $\mathbf{A_{MG}}$ in (25) for three different cases, i.e., the proposed DCVR, the current-based (i.e., I_d–ω and I_q–V) droop control, and the conventional (i.e., P–ω and Q–V) droop control, which are represented by red, green, and blue, respectively. It can be seen that the eigenvalues in the three clusters for the current-based droop control with the state variables $[\Delta I_{odi},\ \Delta I_{oqi}]$ are almost the same as those of the conventional droop control with $[\Delta P_i,\ \Delta Q_i]$. This demonstrates that (2) and (3) can be successfully replaced by (7) and (8), respectively, to take advantage of reducing measurement time delay in practical applications.

In addition, Fig. 4(b) shows that for the proposed DCVR strategy, the eigenvalues in the rightmost cluster move to the left side, compared to those for the current- and power-based droop control strategies. This represents an increase in the system damping and, consequently, an improvement in the small-signal stability of the MG. The comparisons shown in Fig. 4(b) indicate that the dominant poles in the rightmost cluster are sensitive primarily to the state variables $[\Delta I_{odi},\ \Delta I_{oqi}]$ of the proposed I_{dq} controller (or, more accurately, $\mathbf{C_{Pv}}$ in (14), and hence the diagonal elements of $\mathbf{A_{MG}}$ in (A7) in the Appendix), as they are mainly affected by $[\Delta P_i,\ \Delta Q_i]$ in the case of conventional power controllers [6]. Meanwhile, the middle-cluster eigenvalues are sensitive to the state variables of the voltage and current controllers, and the eigenvalues of the left-most cluster are mainly influenced by the state variables of the inverter filters and line currents. The proposed DCVR strategy marginally affects the eigenvalues in both clusters, ensuring overall stability of the MG.

Furthermore, for the proposed DCVR strategy, the root loci of the eigenvalues are analyzed in the case of variations in the I_d–ω and I_q–V droop coefficients (i.e.,m_{Id} and n_{Iq}), while the DCVR coefficient (i.e., n_{Id}) is fixed to 2.42×10^{-1} and 4.84×10^{-1} for 5% and 10% droop gains, respectively. The root loci are then compared to those for the conventional droop control, obtained for variations in m_P and n_Q. Specifically, Fig. 5(a) shows the trajectories of the dominant poles (i.e., part of the low frequency cluster), as m_{Id} and m_P increase from 0.2% to 1% for the proposed and conventional strategies, respectively. The eigenvalues move in the directions corresponding to increase in the absolute magnitudes of their imaginary values. This indicates that, as m_{Id} and m_P increase, the system damping is reduced in both strategies and, consequently, the IDERs become more responsive to variations in the MG frequency and voltage. In the conventional strategy, the eigenvalues move to the right, entering the unstable region (i.e., the right half-plane) for $m_P > 1.82 \times 10^{-4}$. On the contrary, the proposed strategy successfully mitigates the tendency of the MG to become unstable. In particular, in the case of the 10% I_d–V droop gain, a pair of complex conjugate poles only moves a little to the right, and another pair even move to the left. This implies that the proposed DCVR strategy is effective at stabilizing MG operation, for example, when the power outputs of the IDERs happen to change abruptly due to large uncertainties in the frequency droop coefficients in practice.

Similarly, Fig. 5(b) shows the root loci for an increase in n_{Iq} and n_Q from 1% to 11%. The real and complex-conjugate eigenvalues move to the right in both strategies. Specifically, in the conventional strategy, a pair of complex-conjugate eigenvalues moves to the right, eventually entering the unstable region. The tendency is rather mitigated for the proposed one, as in the case shown in Fig. 5(a). The mitigation becomes more noticeable for $n_{Id} = 10\%$. This confirms that the proposed DCVR enables the MG to become more robust against uncertainties in the voltage droop coefficients. Note that for the proposed strategy, the eigenvalues close to the origin move slightly towards the imaginary axis in the beginning, then change direction to the left (see the close-up plot in Fig. 5(b)).

IV. CASE STUDIES AND RESULTS

The MG test bed, shown in Fig. 1, was implemented using Matlab/Simulink to analyze the real-time performance of the proposed DCVR strategy with variation in the load demand,

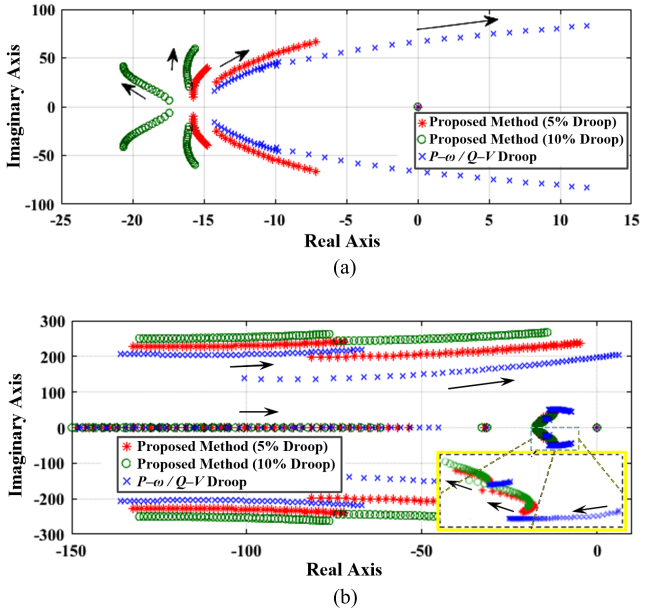

FIGURE 5. Root loci for (a) m_{Id} (and m_P) and (b) n_{Iq} (and n_Q) ranging from 0.2% to 1% and 1% to 11% droop gains, respectively ($2.39 \times 10^{-2} \leq m_{Id} \leq 1.20 \times 10^{-1}$, $6.28 \times 10^{-5} \leq m_P \leq 3.14 \times 10^{-4}$, $2.42 \times 10^{-1} \leq n_{Iq} \leq 2.66$, and $6.35 \times 10^{-4} \leq n_Q \leq 7.00 \times 10^{-3}$).

compared to the conventional P–ω and Q–V droop control (i.e., non-CVR) strategy. The variable load was modelled using (1) to analyze the effects of the power factors and voltage exponents on DCVR performance. For simplicity, the IDERs were modelled using ideal voltage sources, considering the fast dynamic response of the VSI. In (9), n_{Id} and V_n were set to 5% and 1 pu, respectively. The other parameters for the IDERs, lines, and loads remained the same as those used for the small-signal analysis in Section III.

A. PERFORMANCE VALIDATION OF THE PROPOSED DCVR STRATEGY

Fig. 6 shows the profiles of the active and reactive power outputs of the IDERs for stepwise increases in P_{Load} (by 6.55 kW every second); this is equivalent to 50% of the rated power of the constant-impedance loads at Buses 1 and 3. In other words, the variable load consumed 19.65 kW for $t \geq 3$ s, accounting for approximately 60% of the total load demand. The variable load operated with a unity power factor and $n_p = 2$. Fig. 7 shows the corresponding frequency and voltage profiles measured at the output nodes of the IDERs.

Specifically, Fig. 6(a) shows that each IDER generated $P_{IDER} = 4$ kW (or, equivalently, 40% of $P_{IDER,rated} = 10$ kW) during 0.5 s $\leq t \leq$ 1 s. In the proposed DCVR strategy, the I_d–V controller with $n_{Id} = 5\%$ led to decreases in the V_{IDER} levels of the IDERs by approximately 0.02 pu, as shown in Fig. 7(b). As P_{Load} increased during the period 1 s $\leq t \leq$ 4 s, i_{od} increased and ω_{IDER} then decreased in both strategies, as shown in Fig. 7(a); also, see (6) and (7). On the contrary, the V_{IDER} levels were only reduced in the proposed strategy, as shown in Fig. 7(b); see (3) and (9). Fig. 6(a)

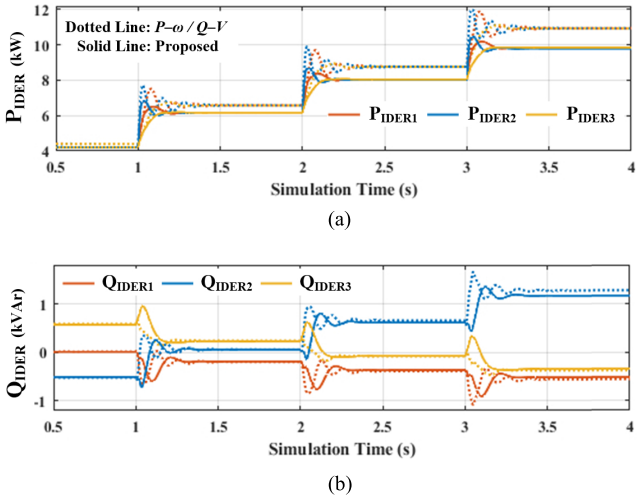

FIGURE 6. (a) Active and (b) reactive power outputs of the IDERs for $n_{Id} = 5\%$.

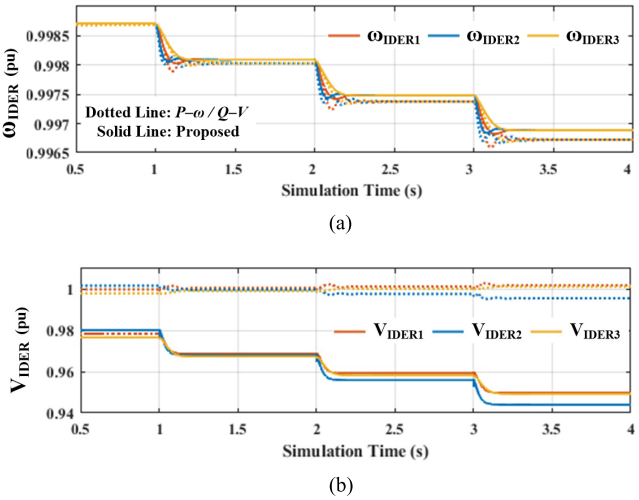

FIGURE 7. (a) Frequency and (b) voltage profiles at the output nodes of the IDERs.

shows that due to the voltage-dependent loads, the total load demand for the proposed strategy became lower than that for the conventional strategy. Therefore, ω_{IDER} deviated less during 1 s $\leq t \leq$ 4 s in the proposed strategy than in the conventional strategy, as shown in Fig. 7(a).

Note that in Fig. 6(b), the I_q–V controllers were as effective as the Q–V controllers at reactive power sharing, This is due to the coupling between the line resistance and reactance, particularly in the case of the small-scale, low-voltage MG [21]. Fig. 7(b) shows that, for the conventional strategy, V_{IDERs} were barely reduced from 1 pu during 1 s $\leq t \leq$ 4 s, because the line power flows and reactive power loads were small. The small changes in V_{IDER} were attributed to variations in the line power flows.

As the MG load demand increased, the output voltages of the IDERs decreased further, as shown in (12). Consequently, a larger decrease in the load demand occured,

TABLE 3. Performance comparisons between the proposed DCVR and the conventional droop control strategy.

	Settling time of $IDER_2$ (s)		Percent overshoot of $IDER_2$ (%)		Load reduction (%)		
Time	1–2 s	2–3 s	1–2 s	2–3 s	1–2 s	2–3 s	3–4 s
Prop.	0.45	0.45	34.2	36.3	6.63	8.62	10.7
Conv.	0.85	0.85	55.7	55.6	0.38	0.44	0.51

TABLE 4. Performance comparisons for different power factors of the variable load.

	Maximum reduction of V (%)	Reduction of P (%)	Reduction of Q (%)
Prop. (unity *pf*)	2.43	8.63	-
Prop. ($pf = 0.9$)	3.25	10.00	10.18
Prop. ($pf = 0.8$)	3.69	10.76	11.02
Conv. (unity *pf*)	0.41	0.42	-
Conv. ($pf = 0.9$)	1.30	2.06	2.22
Conv. ($pf = 0.8$)	1.78	2.90	3.17

as shown in Table 3. This confirms that the proposed strategy is effective for improving the reliability of MG operation by mitigating severe increases in the load demand or, equivalently, the lack of generation reserve capacity. Moreover, the proposed strategy improved the transient response of the IDERs, as shown in Table 3. Specifically, the average percent overshoot and settling time of $IDER_2$ were reduced by approximately 36.7% and 47.1%, respectively, compared to those in the conventional strategy. This is consistent with the results of the eigenvalue analysis, discussed in Section III-B.

B. EFFECTS OF LOAD POWER FACTORS ON THE PROPOSED DCVR

The proposed DCVR strategy was tested for power factors $pf = 1$, 0.9, and 0.8 of the variable load. In other words, Q_{Load} changed by 0, $\pm$6.34 kvar, and $\pm$9.83 kvar, respectively, for a step variation in P_{Load} of $\pm$13.10 kW at $t = 1$ s and 2 s. In (1), both n_p and n_q were set to 2. For each power factor, Figs. 8 and 9 show the variations in the total load demand of the MG and the corresponding profiles of the output voltages of the IDERs, respectively. In Table 4, we summarize the results for the proposed and conventional strategies particularly with respect to the maximum voltage reductions and the decreases in the active and reactive load demands.

For example, the proposed strategy enabled the IDERs to decrease output voltage by up to 3.69% for $pf = 0.8$, in turn reducing the total active and reactive load demands by 10.76% and 11.02%, respectively. In the conventional one, the bus voltages were reduced slightly (i.e., by 1.78%). This demonstrates that the proposed DCVR strategy becomes particularly effective in the case where the MG includes conventional loads (e.g., induction motors and home appliances [38]) operating with relatively low power factors by consuming reactive power.

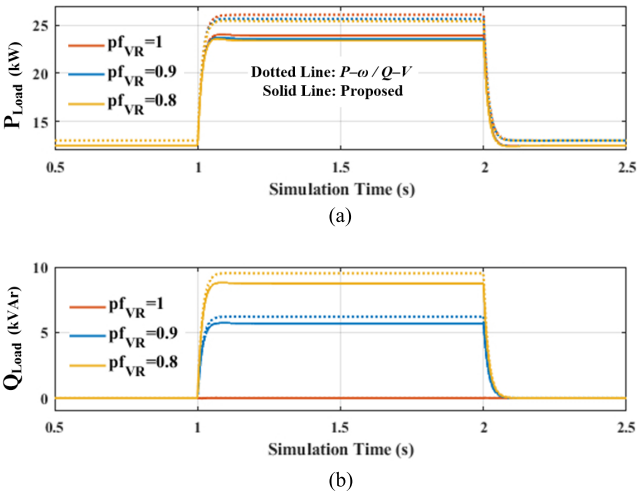

FIGURE 8. Total (a) active and (b) reactive load demands for different *pf*s.

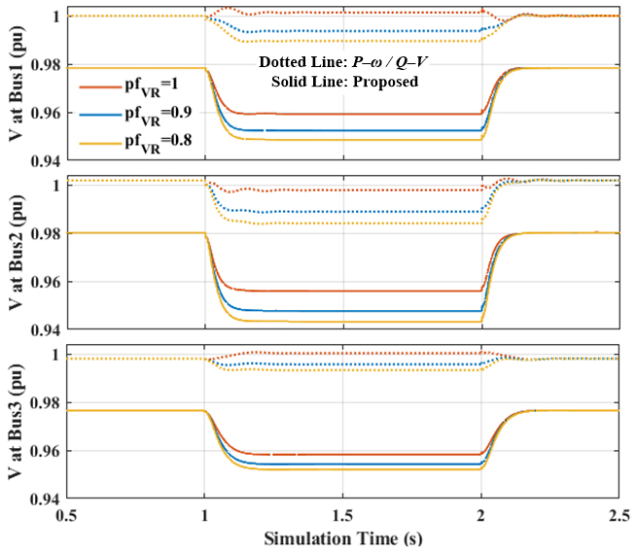

FIGURE 9. Output voltage profiles of the IDERs for different *pf*s.

Moreover, in both strategies, the lower the power factor, the greater the decreases in the output voltage, and consequently, the total load demand due to the I_q–V and Q–V controllers for reactive power sharing. This implies that n_{Id} and n_{Iq} must be determined based on the operating power factors of the loads to improve the DCVR performance while ensuring the voltage stability.

C. EFFECTS OF LOAD COMPOSITIONS ON THE PROPOSED DCVR

The case study, discussed in Section IV-B, was repeated with different values of n_p in (1) to analyze the effects of the voltage dependence of the variable load on the proposed DCVR strategy. Specifically, the analysis was conducted for $n_p = 2$, 1, and 0, representing the variable load being operated as a constant-impedance, current, and power load, respectively.

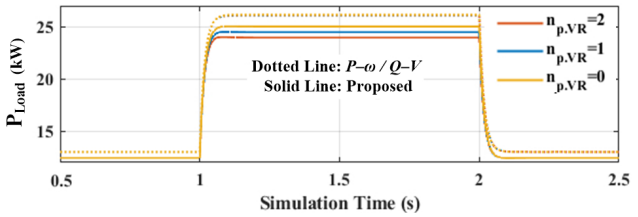

FIGURE 10. Total active load demand in the MG for different values of n_p in (1).

TABLE 5. Performance comparisons for different voltage exponents of the variable load.

	Equivalent voltage exponent, $n_{p.eq}$	Maximum reduction of V (%)	Reduction of P (%)
Prop. ($n_p = 2$)	2	2.42	8.62
Prop. ($n_p = 1$)	1.5	2.54	6.65
Prop. ($n_p = 0$)	1	2.66	4.48
Conv.	2	0.41	0.42

As the variable load consumed as much power P_{Load} as half of the total load demand in the MG, the equivalent voltage exponent $n_{p.eq}$ for the total MG load was estimated as 2, 1.5, and 1, respectively. Note that Q_{Load} was set to zero: i.e., $pf = 1$.

Figs. 10 and 11 show the variations in total load demand and bus voltages, respectively, for step changes in P_{Load}. Table 5 shows that for the proposed strategy, bus voltage was reduced by up to 0.956, 0.955, and 0.954 pu (i.e., by up to 2.42%, 2.54%, and 2.66%) for $n_{p.eq} = 2$, 1.5, and 1, respectively. This led to a reduction in the total load demand

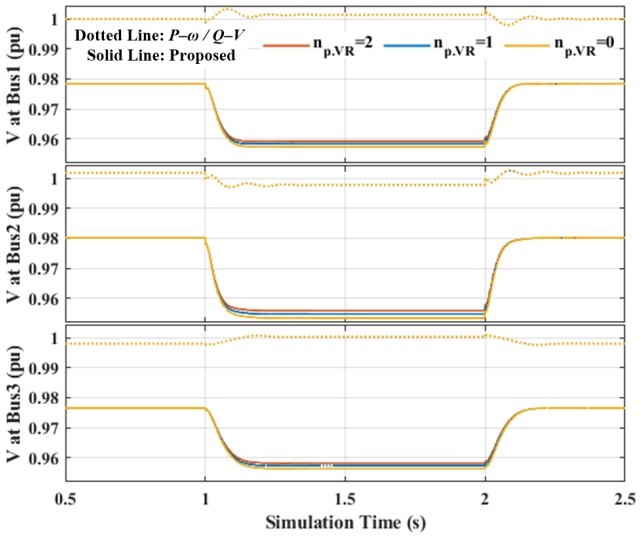

FIGURE 11. Bus voltage profiles for different values of n_p in (1).

of 2.26 kW, 1.74 kW, and 1.17 kW (i.e., 8.62%, 6.65%, and 4.48%), respectively. In other words, the larger the value of $n_{p,eq}$, the larger the reduction in the load demand. This confirms that the proposed DCVR strategy is effective for reducing the total load demand particularly for the case where the constant-impedance loads account for large proportion of the load. In contrast, the conventional droop control led to small variations in bus voltage for the changes in P_{Load}, due to $Q_{Load} = 0$, as in Section IV-B. Fig. 11 also shows that the

$$\mathbf{T_{Si}} = \begin{bmatrix} \cos\delta_i & -\sin\delta_i \\ \sin\delta_i & \cos\delta_i \end{bmatrix}, \quad \mathbf{T_{Ci}} = \begin{bmatrix} -i_{odi}\sin\delta_i & -i_{oqi}\cos\delta_i \\ i_{odi}\cos\delta_i & i_{oqi}\sin\delta_i \end{bmatrix} \tag{A1}$$

$$\mathbf{T_{Vi}^{-1}} = \begin{bmatrix} -v_{bDi}\sin\delta_i + v_{bQi}\cos\delta_i \\ v_{bDi}\cos\delta_i - v_{bQi}\sin\delta_i \end{bmatrix} \tag{A2}$$

$$\mathbf{A_{INVi}} = \begin{bmatrix} \mathbf{A_{Pi}} & \mathbf{0} & \mathbf{0} & \mathbf{B_{Pi}} \\ \mathbf{B_{V1i}C_{Pvi}} & \mathbf{0} & \mathbf{0} & \mathbf{B_{V2i}} \\ \mathbf{B_{V1i}D_{V1i}C_{Pvi}} & \mathbf{B_{C1i}C_{Vi}} & \mathbf{0} & \mathbf{B_{C1i}D_{V2i}+B_{C2i}} \\ \mathbf{B_{LCL1i}D_{C1i}D_{V1i}C_{Pvi}} \\ \mathbf{+B_{LCL2i}}\begin{bmatrix} \mathbf{T_{Vi}^{-1}} & \mathbf{0} \end{bmatrix} \\ \mathbf{+B_{LCL3i}C_{P\omega i}} & \mathbf{B_{LCL1i}D_{C1i}C_{Vi}} & \mathbf{B_{LCL1i}C_{Ci}} & \mathbf{A_{LCLi}+} \\ & & & \mathbf{B_{LCL1i}}\begin{pmatrix} \mathbf{D_{C1i}D_{V2i}} \\ \mathbf{+D_{C2i}} \end{pmatrix} \end{bmatrix}_{13\times 13}, \tag{A3}$$

$$\mathbf{A_{INV}} = \begin{bmatrix} \mathbf{A_{INV1}+X_{m_p}} & \mathbf{0} & \mathbf{0} & \cdots & \mathbf{0} \\ \mathbf{X_{m_p}} & \mathbf{A_{INV2}} & \mathbf{0} & \cdots & \mathbf{0} \\ \mathbf{X_{m_p}} & \mathbf{0} & \ddots & \ddots & \vdots \\ \vdots & \vdots & \ddots & \ddots & \mathbf{0} \\ \mathbf{X_{m_p}} & \mathbf{0} & \cdots & \mathbf{0} & \mathbf{A_{INVk}} \end{bmatrix}_{13k\times 13k}, \quad \mathbf{X_{m_p}} = \begin{bmatrix} \begin{bmatrix} \mathbf{C_{P\omega j}} & \mathbf{0} \end{bmatrix} \\ \mathbf{0} \end{bmatrix}_{13\times 13}, \tag{A4}$$

$$\mathbf{B_{INVi}} = \begin{bmatrix} \mathbf{0} \\ \mathbf{B_{LCL2i}T_{Si}^{-1}} \end{bmatrix}_{13\times 2}, \quad \mathbf{B_{INV\omega i}} = \begin{bmatrix} \mathbf{B_{P\omega}} \\ \mathbf{0} \end{bmatrix}_{13\times 1}, \quad \mathbf{C_{INVci}} = [\,\mathbf{T_{Ci}} \quad \mathbf{0} \quad \mathbf{T_{Si}}\,]_{2\times 13},$$

$$\mathbf{C_{INV\omega i}} = \begin{cases} [\,\mathbf{C_{P\omega i}} \quad \mathbf{0}\,]_{1\times 13} & i = 1 \\ [\mathbf{0}]_{1\times 13} & i \neq 1, \end{cases} \tag{A5}$$

$$\mathbf{B_{INV}} = diag([\mathbf{B_{INV1}}, \mathbf{B_{INV2}}, \cdots, \mathbf{B_{INVk}}])_{13k\times 2m}, \mathbf{C_{INV}} = diag([\mathbf{C_{INVc1}}, \mathbf{C_{INVc2}}, \cdots, \mathbf{C_{INVck}}])_{2k\times 13k}, \tag{A6}$$

$$\mathbf{A_{MG}} = \begin{bmatrix} \mathbf{A_{INV}+B_{INV}R_NM_{INV}C_{INV}} & \mathbf{B_{INV}R_NM_{NET}} & \mathbf{B_{INV}R_NM_{LOAD}} \\ \mathbf{B_{1NET}R_NM_{INV}C_{INVc}+B_{2NET}C_{INV\omega}} & \mathbf{A_{NET}+B_{1NET}R_NM_{NET}} & \mathbf{B_{1NET}R_NM_{LOAD}} \\ \mathbf{B_{1LOAD}R_NM_{INV}C_{INVc}+B_{2LOAD}C_{INV\omega}} & \mathbf{B_{1LOAD}R_NM_{NET}} & \mathbf{A_{LOAD}+B_{1LOAD}R_NM_{LOAD}} \end{bmatrix}_{(13k+2n+2p)\times(13k+2n+2p)}. \tag{A7}$$

voltage profile at each bus remained the same for $n_p = 2$, 1, and 0.

V. CONCLUSION

This paper proposed a new DCVR strategy incorporated with current-based droop control to improve the operational reliability of an inverter-based islanded MG. For the proposed DCVR, the I_{dq} controller was developed as the outer feedback controller of the IDER, requiring no communications systems. The I_{dq} controller consists of an I_d–V controller for the DCVR, and I_d–ω and I_q–V controllers for power sharing. The I_d–V controllers adjusted the voltage outputs of the individual IDERs in proportion to the MG frequency variation, mainly determined by the I_d–ω controllers. In other words, decentralized operation of the IDERs could be achieved using the global signal in the MG, so that the local controllers of the IDERs reduced output voltage while maintaining the overall profile of the original voltage at the MG buses. The I_q–V controllers, integrated with the I_d–V controllers, also adjusted IDER voltage for reactive power sharing. The proposed I_{dq} controller enabled the IDERs to respond faster to variations in the load demand, thus improving the transient responses of the IDERs. A state-space model of the three-bus MG test bed was implemented so that the small-signal analysis could be performed particularly for variations in m_{Id} and n_{Iq}. The proposed DCVR was shown to increase the system damping, and consequently the reliability of the MG operation. Case studies were also performed to demonstrate that, with an increase in load demand, the proposed DCVR led to larger reductions in bus voltages and, consequently, in the power inputs of the constant-impedance loads, resulting in larger system damping. The proposed DCVR was also confirmed to be effective for an MG that includes large constant impedance loads operating with relatively low power factors.

APPENDIX

The state space model of the MG test bed, discussed in Section III-A, is implemented using the transformation matrices (A1) and (A2), as shown at the bottom of the previous page, and the coefficient matrices (A3)–(A7), as shown at the bottom of the previous page, the elements of which are comprehensively explained in [6].

REFERENCES

[1] N. Hatziargyriou, *Microgrids: Architectures and Control*. Hoboken, NJ, USA: Wiley, 2014.

[2] M. A. Hossain, H. R. Pota, M. J. Hossain, and F. Blaabjerg, "Evolution of microgrids with converter-interfaced generations: Challenges and opportunities," *Int. J. Elect. Power Energy Syst.*, vol. 109, pp. 160–186, Jul. 2019.

[3] B. Kroposki, C. Pink, R. DeBlasio, H. Thomas, M. Simões, and P. K. Sen, "Benefits of power electronic interfaces for distributed energy systems," *IEEE Trans. Energy Convers.*, vol. 25, no. 3, pp. 901–908, Sep. 2010.

[4] X. Lu and J. Wang, "A game changer: Electrifying remote communities by using isolated microgrids," *IEEE Electrific. Mag.*, vol. 5, no. 2, pp. 56–63, Jun. 2017.

[5] Q.-C. Zhong, "Power-electronics-enabled autonomous power systems: Architecture and technical routes," *IEEE Trans. Ind. Electron.*, vol. 64, no. 7, pp. 5907–5918, Jul. 2017.

[6] N. Pogaku, M. Prodanovic, and T. C. Green, "Modeling, analysis and testing of autonomous operation of an inverter-based microgrid," *IEEE Trans. Power Electron.*, vol. 22, no. 2, pp. 613–625, Mar. 2007.

[7] T. C. Green and M. Prodanovic, "Control of inverter-based micro-grids," *Electr. Power Syst. Res.*, vol. 77, no. 9, pp. 1204–1213, Jul. 2007.

[8] A. G. Tsikalakis and N. D. Hatziargyriou, "Centralized control for optimizing microgrids operation," in *Proc. IEEE Power Energy Soc. Gen. Meeting*, Detroit, MI, USA, Jul. 2011, pp. 1–8.

[9] D. E. Olivares, C. A. Cañizares, and M. Kazerani, "A centralized energy management system for isolated microgrids," *IEEE Trans. Smart Grid*, vol. 5, no. 4, pp. 1864–1875, Jul. 2014.

[10] D. E. Olivares, A. Mehrizi-Sani, A. H. Etemadi, C. A. Cañizares, R. Iravani, M. Kazerani, A. H. Hajimiragha, O. Gomis-Bellmunt, M. Saeedifard, R. Palma-Behnke, G. A. Jiménez-Estévez, and N. D. Hatziargyriou, "Trends in microgrid control," *IEEE Trans. Smart Grid*, vol. 5, no. 4, pp. 1905–1919, Jul. 2014.

[11] S. Parhizi, H. Lotfi, A. Khodaei, and S. Bahramirad, "State of the art in research on microgrids: A review," *IEEE Access*, vol. 3, pp. 890–925, 2015.

[12] A. Kaur, J. Kaushal, and P. Basak, "A review on microgrid central controller," *Renew. Sustain. Energy Rev.*, vol. 55, pp. 338–345, Mar. 2016.

[13] M. C. Chandorkar, D. M. Divan, and R. Adapa, "Control of parallel connected inverters in standalone AC supply systems," *IEEE Trans. Ind. Appl.*, vol. 29, no. 1, pp. 136–143, Jan./Feb. 1993.

[14] J. A. P. Lopes, C. L. Moreira, and A. G. Madureira, "Defining control strategies for microgrids islanded operation," *IEEE Trans. Power Syst.*, vol. 21, no. 2, pp. 916–924, May 2006.

[15] I.-Y. Chung, W. Liu, D. A. Cartes, E. G. Collins, and S.-I. Moon, "Control methods of inverter-interfaced distributed generators in a microgrid system," *IEEE Trans. Ind. Appl.*, vol. 46, no. 3, pp. 1078–1088, May/Jun. 2010.

[16] X. Hou, Y. Sun, J. Lu, X. Zhang, L. H. Koh, M. Su, and J. M. Guerrero, "Distributed hierarchical control of AC microgrid operating in grid-connected, islanded and their transition modes," *IEEE Access*, vol. 6, pp. 77388–77401, 2018.

[17] Y. Khayat, M. Naderi, Q. Shafiee, Y. Batmani, M. Fathi, J. M. Guerrero, and H. Bevrani, "Decentralized optimal frequency control in autonomous microgrids," *IEEE Trans. Power Syst.*, vol. 34, no. 3, pp. 2345–2353, May 2019.

[18] J. Kim, J. M. Guerrero, P. Rodriguez, R. Teodorescu, and K. Nam, "Mode adaptive droop control with virtual output impedances for an inverter-based flexible AC microgrid," *IEEE Trans. Power Electron.*, vol. 26, no. 3, pp. 689–701, Mar. 2011.

[19] M. B. Delghavi and A. Yazdani, "An adaptive feedforward compensation for stability enhancement in droop-controlled inverter-based microgrids," *IEEE Trans. Power Del.*, vol. 26, no. 3, pp. 1764–1773, Jul. 2011.

[20] M. S. Golsorkhi and D. D. C. Lu, "A control method for inverter-based islanded microgrids based on V-I droop characteristics," *IEEE Trans. Power Del.*, vol. 30, no. 3, pp. 1196–1204, Jun. 2015.

[21] Y. Han, H. Li, P. Shen, E. A. A. Coelho, and J. M. Guerrero, "Review of active and reactive power sharing strategies in hierarchical controlled microgrids," *IEEE Trans. Power Electron.*, vol. 32, no. 3, pp. 2427–2451, Mar. 2017.

[22] H. Dong, S. Yuan, Z. Han, X. Ding, S. Ma, and X. Han, "A comprehensive strategy for power quality improvement of multi-inverter-based microgrid with mixed loads," *IEEE Access*, vol. 6, pp. 30903–30916, 2018.

[23] R. M. Imran, S. Wang, and F. M. F. Flaih, "DQ-voltage droop control and robust secondary restoration with eligibility to operate during communication failure in autonomous microgrid," *IEEE Access*, vol. 7, pp. 6353–6361, 2018.

[24] Z. Afshar, M. Mollayousefi, S. M. T. Bathaee, M. T. Bina, and G. B. Gharehpetian, "A novel accurate power sharing method versus droop control in autonomous microgrids with critical loads," *IEEE Access*, vol. 7, pp. 89466–89474, 2019.

[25] R. F. Preiss and V. J. Warnock, "Impact of voltage reduction on energy and demand," *IEEE Trans. Power App. Syst.*, vol. PAS-97, no. 5, pp. 1665–1671, Sep. 1978.

[26] D. M. Lauria, "Conservation Voltage Reduction (CVR) at Northeast Utilities," *IEEE Trans. Power Del.*, vol. PWRD-2, no. 4, pp. 1186–1191, Oct. 1987.

[27] A. Dwyer, R. E. Nielsen, J. Stangl, and N. S. Markushevich, "Load to voltage dependency tests at B.C. Hydro," *IEEE Trans. Power Syst.*, vol. 10, no. 2, pp. 709–715, May 1995.

[28] Z. Wang and J. Wang, "Review on implementation and assessment of conservation voltage reduction," *IEEE Trans. Power Sys.*, vol. 29, no. 3, pp. 1306–1315, May 2014.
[29] P. K. Sen and K. H. Lee, "Conservation voltage reduction technique: An application guideline for smarter grid," *IEEE Trans. Ind. Appl.*, vol. 52, no. 3, pp. 2122–2128, May/Jun. 2016.
[30] K.-S. Shim, S.-I. Go, S.-Y. Yun, J.-H. Choi, W. Nam-Koong, C.-H. Shin, and S.-J. Ahn, "Estimation of conservation voltage reduction factors using measurement data of KEPCO system," *Energies*, vol. 10, no. 12, p. 2148, Dec. 2017.
[31] M. Gheydi, A. Nouri, and N. Ghadimi, "Planning in microgrids with conservation of voltage reduction," *IEEE Syst. J.*, vol. 12, no. 3, pp. 2782–2790, Sep. 2018.
[32] M. Farrokhabadi, C. A. Cañizares, and K. Bhattacharya, "Frequency control in isolated/islanded microgrids through voltage regulation," *IEEE Trans. Smart Grid*, vol. 8, no. 3, pp. 1185–1194, May 2017.
[33] A. M. Pasha, H. H. Zeineldin, A. S. Al-Sumaiti, M. S. E. Moursi, and E. F. E. Sadaany, "Conservation voltage reduction for autonomous microgrids based on V–I droop characteristics," *IEEE Trans. Sustain. Energy*, vol. 8, no. 3, pp. 1076–1085, Jul. 2017.
[34] A. Aderibole, H. H. Zeineldin, M. Al Hosani, and E. F. El-Saadany, "Demand side management strategy for droop-based autonomous microgrids through voltage reduction," *IEEE Trans. Energy Convers.*, vol. 34, no. 2, pp. 878–888, Jun. 2019.
[35] S. Leitner, M. Yazdanian, A. Mehrizi-Sani, and A. Muetze, "Small-signal stability analysis of an inverter-based microgrid with internal model-based controllers," *IEEE Trans. Smart Grid*, vol. 9, no. 5, pp. 5393–5402, Sep. 2018.
[36] P. Kundur, *Power System Stability and Control* (The Epri Power System Engineering). New York, NY, USA: McGraw-Hill, 1994.
[37] A. Arif, Z. Wang, J. Wang, B. Mather, H. Bashualdo, and D. Zhao, "Load modeling—A review," *IEEE Trans. Smart Grid*, vol. 9, no. 6, pp. 5986–5999, Nov. 2018.
[38] A. Bokhari, A. Alkan, R. Dogan, M. Diaz-Aguiló, F. de León, D. Czarkowski, Z. Zabar, L. Birenbaum, A. Noel, and R. E. Uosef, "Experimental determination of the ZIP coefficients for modern residential, commercial, and industrial loads," *IEEE Trans. Power Del.*, vol. 29, no. 3, pp. 1372–1381, Jun. 2014.

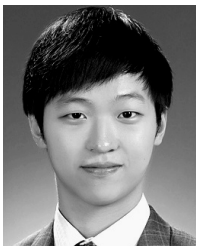

HYEON-JIN MOON (S'17) received the B.S. degree in electrical and control engineering from Hanyang University, Seoul, South Korea, in 2012. He is currently pursuing the Ph.D. degree in electrical engineering with Seoul National University, Seoul.

His research interests include power system control, islanded microgrids, distributed energy resources, and decentralized power management.

YOUNG-JIN KIM (S'14–M'15) received the B.S. and M.S. degrees from Seoul National University, in 2007 and 2010, respectively, and the Ph.D. degree from the Massachusetts Institute of Technology, in 2015, all in electrical engineering.

He was a Visiting Scholar with the Catalonia Institute for Energy Research, in 2014, and a Postdoctoral Researcher with the Argonne National Laboratory, Energy Systems Division, Center for Energy, Environmental, and Economic Systems Analysis, from 2015 to 2016. He joined the Pohang University of Science and Technology (POSTECH), as a Faculty Member, where he is currently an Assistant Professor with the Department of Electrical Engineering. His research interests include distributed generators, renewable energy resources, and smart buildings.

Dr. Kim is an Editor of the IEEE TRANSACTIONS ON SMART GRID.

SEUNG-IL MOON (M'93–SM'14) received the B.S. degree from Seoul National University, Seoul, South Korea, in 1985, and the M.S. and Ph.D. degrees from Ohio State University, Columbus, in 1989 and 1993, respectively, all in electrical engineering.

He is currently a Professor with the School of Electrical Engineering and Computer Science, Seoul National University. His research interests include power system operation, power quality, flexible ac transmission systems, renewable energy, and distributed generation.

Dr. Moon has received many awards and honors, include the Service Merit Medal (Korean Government), the Young-Moon Park Best Scholar Award, and the Outstanding Scholar Award (Korean Institute of Electrical Engineers).